International Journal of Fatigue 152 (2021) 106450

Contents lists available at ScienceDirect

International Journal of Fatigue

journal homepage: www.elsevier.com/locate/ijfatigue

Reliability analysis of fatigue crack growth for rail steel under variable amplitude service loading conditions and wear

Reza Masoudi Nejad [a,*], Zhiliang Liu [a], Wenchen Ma [b], Filippo Berto [c]

[a] School of Mechanical and Electrical Engineering, University of Electronic Science and Technology of China, Chengdu 611731, China
[b] Department of Civil and Environmental Engineering and Construction, University of Nevada, Las Vegas, 4505 S. Maryland Parkway, Las Vegas, NV 89154, USA
[c] Department of Mechanical and Industrial Engineering, NTNU – Norwegian University of Science and Technology, Trondheim, Norway

ARTICLE INFO

Keywords:
Fatigue crack growth
Fatigue reliability
Wear
Variable amplitude
Multiple site crack

ABSTRACT

The purpose of this paper is to investigate the effect of variable amplitude service loading conditions and wear phenomenon on reliability analysis for rail steel. For this purpose, the rail with the exact geometry of the profile in the railway systems and the boundary element method has been used. Also, the geometry correction functions of the five cracks, as a function of a crack size are determined by using nonlinear regression analysis estimating the statistical descriptors of the five geometry correction functions. Fatigue reliability is evaluated for each failure mode due to multiple site fatigue cracks propagation in rail steel.

1. Introduction

It is quite difficult to calculate the combined stress conditions that result in the termination of elastic and inelastic deformations, that is, predicting the failure of a material is quite difficult. Masoudi Nejad et al. [1] showed that as cyclic loading continued, deeper troughs gradually began to arise from random slippage (based on statistical formulation). Lin and Ito [2] calculated the relative motion of two adjacent planes. Calculations with acceptable hypotheses showed that the local plastic shear strain on both plates (one positive and the other negative) may reach a high value in a small number of cycles. This high plastic strain causes the layers between the plates to come out or sink. In other hands, in the second case, we have continuous deepening of the depressions. The Lynch model [3] gives similar results, assuming that the soft layers come in and out during cyclic loading. The Dang Van multiaxial fatigue criterion has been suggested in a simple approximate formulation by Ekberg et al. [4]. Ciavarella et al., it was found that the approximation is only valid in a restricted range of cases [5]. Ciavarella and Monno [6] compared the Dang Van criterion for RCF with one integral approach criterion (Papadopoulos) and the more classical Crossland criterion. Desimone et al. [7] studied the problem of the calibration of the Dang Van multiaxial fatigue criterion. The stress–strain response of the material around the crack tip and the microstructural factors of the material determine the crack behavior under loading conditions [8–10]. After this initial acceleration, the crack growth rate decreases rapidly and reaches a minimum after a small number of fatigue cycles [11–13]. In order to ensure the movement of the train on the rails, Kim et al. [14] evaluated the behavior of the steel rail under mixed-mode loading condition. To obtain these results, stress analysis was performed under static load and cyclic load and the results of stress analysis indicated that the crack progresses to the depth, it is increasing. Skatebel et al. [15] examined the fatigue crack growth in the railway rail under the influence of the residual stresses due to welding. Considering the effect of residual stresses, they investigated the effect of railway wheel passage on fatigue crack growth by finite element method. Bertha et al. [16] showed that cracks initially begin to grow parallel to the surface of the rail, but after a while tend to grow in depth. They examined the fatigue crack growth process and growth path determination, two important factors in determining rail inspection intervals. Ekberg et al. [17] investigated the deterioration in the form of RCF of wheels and rails with the aim of putting RCF prediction and prevention in context. Afferrante et al. [18] investigated a re-interpretation of recent ratchetting measurements by Clayton and Su [19] shows evidence of ratchetting as the mechanism dominating in RCF fatigue. Reliability assessment in the fatigue of welded structures is a significant issue for the development of probability methods. These methods [20,21] discuss the uncertainty in loading the reaction and the strength of the structure as a random variable. By combining the load distribution and the strength distribution of the structure, the probability of its failure is calculated by a suitable

* Corresponding author.
E-mail addresses: masoudinejad@uestc.edu.cn (R. Masoudi Nejad), zhiliang_liu@uestc.edu.cn (Z. Liu), maw2@unlv.nevada.edu (W. Ma), filippo.berto@ntnu.no (F. Berto).

https://doi.org/10.1016/j.ijfatigue.2021.106450
Received 26 June 2021; Received in revised form 20 July 2021; Accepted 25 July 2021
Available online 29 July 2021

Nomenclature

$\frac{da}{dN}$	crack growth rate
da	crack extension length
dN	cycle jump
ΔK	stress intensity factor range
K	stress intensity factor
K_I	stress intensity factor of mode-I
$K_{I\,max}$	maximum stress intensity factor of mode-I
K_C	stress intensity factor due to an offset loaded hole
f_I	non-dimensional factor
β	geometric correction factor
$\beta(t)$	reliability index
β_i	reliability indices corresponding to the ith
β_j	reliability indices corresponding to the jth
ρ_{ij}	correlation coefficient between the ith and jth component failure
υ	long-term average response frequency
$\phi_2(\cdot)$	probability density function
Φ	standardized normal distribution
$\Phi_2(\cdot)$	cumulative distribution function
σ	stress
a	crack length
a_0	Length of the open portion of the crack
a_f	final crack length
a_{max}	Maximum crack length
A	regression parameter
B	regression parameter
C	parameter in the crack growth model
$E[a(t)]$	mean value of crack length
$E(\Delta\sigma)$	mean value of applied stress range
$E(A)$	mean value of parameter A
$E(B)$	mean value of parameter B
$E(C)$	mean value of parameter C
i	represents the crack tip number
L	length of ship
m	parameter in the crack growth model
N	number of cycles
$P_{f,i}$	probability of failure corresponding to the ith failure mode
$P(U)$	failure probability of the series system
R	load ratio
$R(t)$	reliability
S	standard deviation of crack length
S_{a_0}	standard deviation of initial crack length
$S_{\Delta\sigma}$	standard deviation of applied stress range
S_A	standard deviation of parameter A
S_B	standard deviation of parameter B
S_C	standard deviation of parameter C
t	time
SIFs	stress intensity factors
BEM	boundary element method
FEM	finite element method
XFEM	extended finite element method
GFDM	generalized finite difference method
GFEM	generalized finite element method
EFG	element-free Galerkin method
VPM	virtual-node polygonal finite element method
BES	boundary element solver
MTS	maximum tangential stress

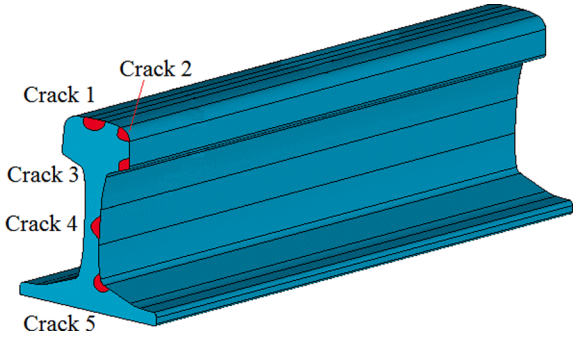

Fig. 1. Fatigue cracks in the Grade 900A rail steel.

Table 1
Mechanical properties of railway wheel and rail [50].

Component	Elastic module (GPa)	Poisson's ratio	Yield stress (MPa)
Wheel	205	0.3	527
Rail	206.9	0.295	483

method. In this way, the accumulation of fatigue failure is considered as a random variable [22–26]. Random means the loading process and the fatigue strength of the material. Avontuur and Van der Werff [27] proposed an algorithm based on the finite element method that is implemented to analyze the reliability of mechanical structures in the software. They showed that finite element approximation is suitable for analyzing the reliability of mechanical drive systems. Jessus et al. [28] proposed a model for estimation of probabilistic fatigue S–N curves for

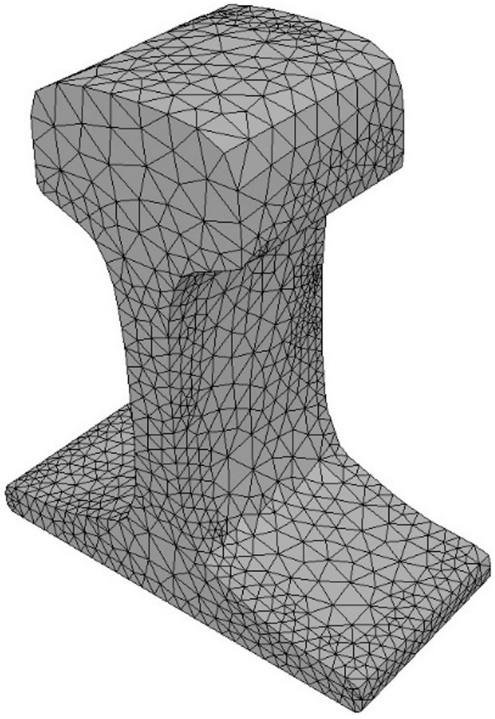

Fig. 2. Boundary element modeling of rail steel.

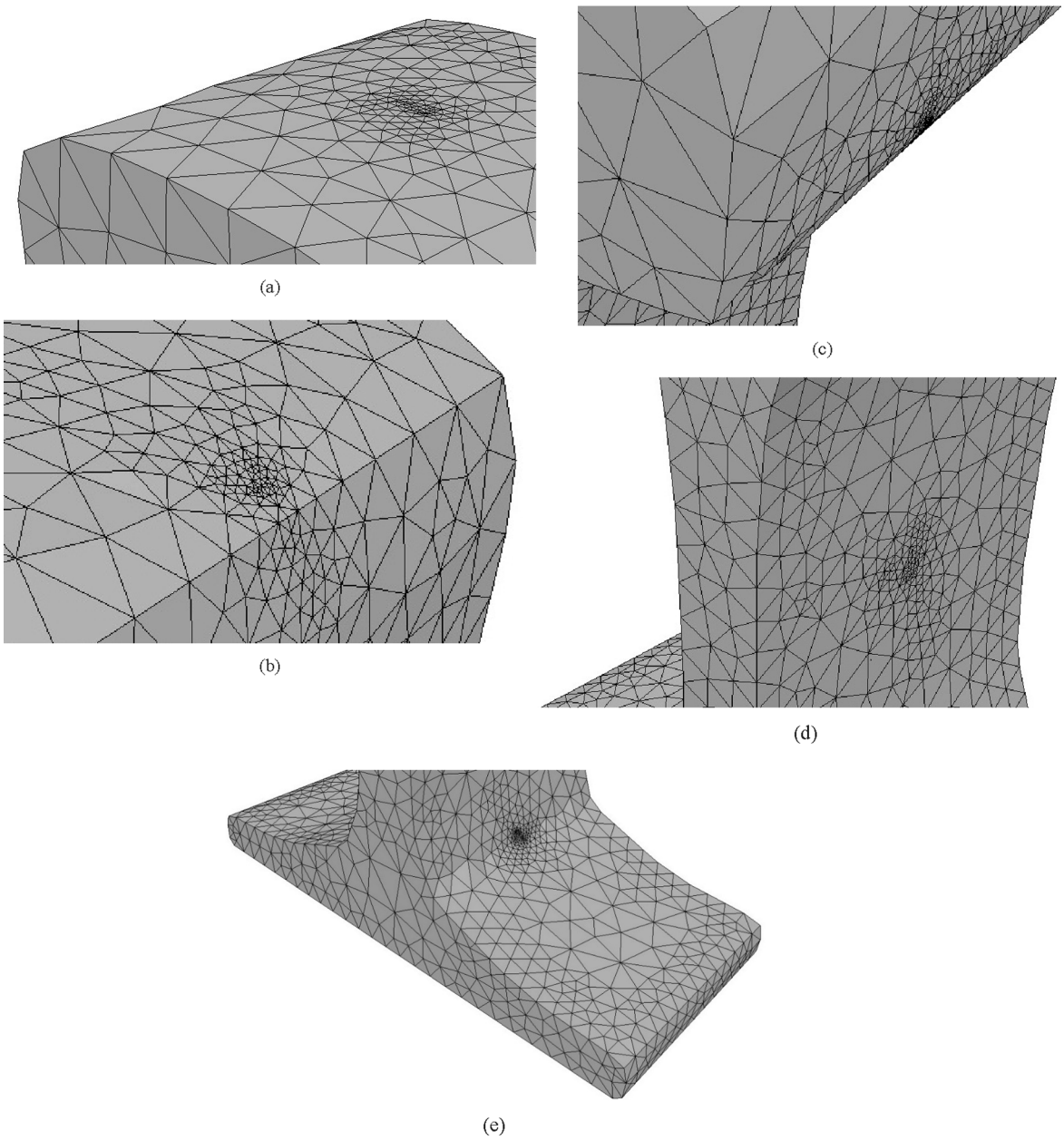

Fig. 3. Crack position and configuration; a) Crack 1, b) Crack 2, c) Crack 3, d) Crack 4, and e) Crack 5.

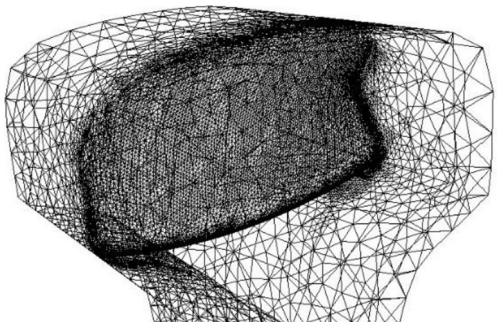

Fig. 4. Fatigue crack growth with BEM for first mode failure.

notched structural components. They used a simplified elastoplastic analysis based on the Neuber and the Glinka rules which were supported by the results of an elastic finite element analysis of the riveted connection. Inspection scheduling is seen in many reliability applications [29–33]. The best method of maintenance scheduling can be expressed as an assessment between the costs associated with inspection and repair and the level of reliability [34–36]. Zhao et al. [37] evaluated the reliability and optimization of inspection time for a component with multiple defects. This inspection identifies any defects. An algorithm was proposed to optimize inspection intervals to increase the reliability of this component. Boundary element method appears to be an efficient algorithm when simulating the cracking problems, and nevertheless other numerical methods such as finite element method (FEM), element-free Galerkin method (EFG) and the generalized finite element method (GFEM) [38–41]. A new computational technique, known as element-free Galerkin method (EFG), proposed by Brighenti [42]. Wu et al. used novel extended finite element method (XFEM) and virtual-node polygonal finite element method (VPM) approaches to conduct the thermal fatigue crack growth analysis and life evaluation [43]. Song et al. investigated the development and the application of the scaled boundary finite element method for fracture analysis [44]. Jiang et al.

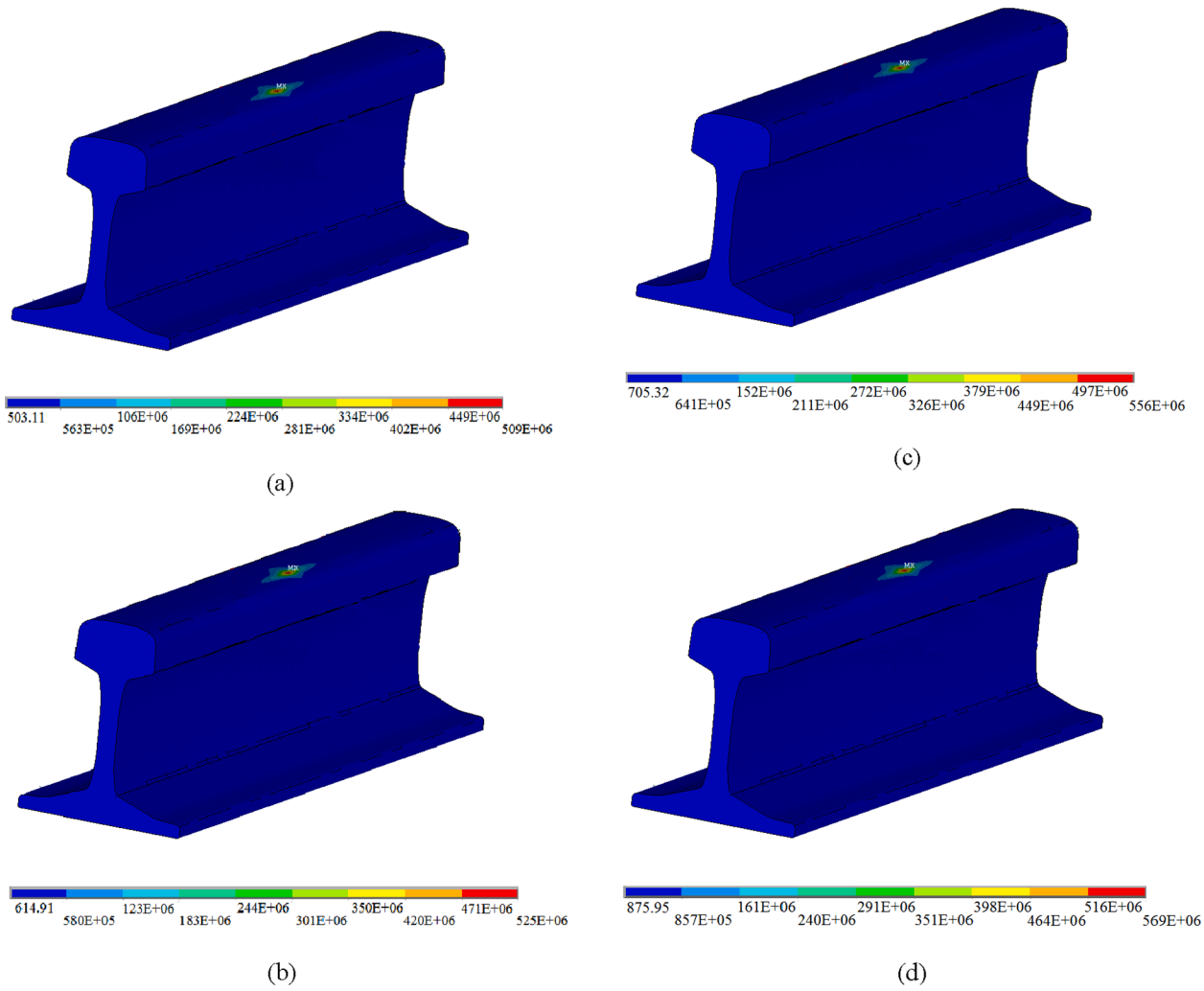

Fig. 5. Stress distribution for the wheel/rail contact, a) new wheel profile, b) first type of worn wheel, c) second type of worn wheel, d) third type of worn wheel.

investigate the first attempt to apply the generalized finite difference method (GFDM), a recently developed meshless collocation method, for fracture mechanics analysis of dissimilar elastic materials with interfacial cracks [45].

In some of the studies, cracks have been propagated and new wheel and rail profiles have been considered. In this paper, by considering the parameters in the railway system, first the maximum stress on the rail during contact with the wheel is simulated. Then the results were used as input for the fatigue crack growth under the influence of variable amplitude service loading conditions. According to field observations, five cracks are initiated and propagated at critical points. Stress intensity factors at the tip of cracks are calculated by boundary element method, considering all possible combinations of all cracks of different lengths. Paris Equation is used as a criterion of the fatigue crack growth rate and the maximum tangential stress was considered as the crack growth direction. Also, Morgan law is used to describe the failure probability of the series system.

2. Proposed model for fatigue reliability assessment

The fatigue crack growth depends on a significant number of complex variables. After years of research, the impact of factors such as the specimen size, the specimen geometry, the loading conditions, the material properties and the environmental factors on the fatigue crack growth is still not fully understood. The fatigue crack growth rate depends on the minimum and maximum stress intensity factors. The relation for fatigue crack growth rate as a function is [46]:

$$\frac{da}{dN} = f_I(\Delta K, R), \tag{1}$$

where R is load ratio and $\Delta K$is stress intensity factor range.

By integrating Eq. (1) for the growth of a crack from the initial length a_0 to the final length a_f, Eq. (2) is obtained:

$$N = \int_{a_0}^{a_f} \frac{da}{f_I(\Delta K, R)}. \tag{2}$$

The Paris law is used to describe the fatigue crack growth behavior and to predict the fatigue life under cyclic loading to failure in accordance with Eq. (3) [47–51]:

$$\frac{da}{dN} = C(\Delta K)^m, \tag{3}$$

where C, m are material constants.

The stress intensity factor for a crack can be calculated from Eq. (4):

$$K = \beta\sigma\sqrt{\pi a}, \tag{4}$$

where a is crack length, $\sigma$is the stress applied to specimen, K is the stress intensity factor and β is the geometric correction factor.

With Eqs. (3) and (4) we obtain:

$$\frac{da}{dN} = C(\beta\Delta\sigma\sqrt{\pi a})^m = C\beta^m\Delta\sigma^m(\pi a)^{\frac{m}{2}}. \tag{5}$$

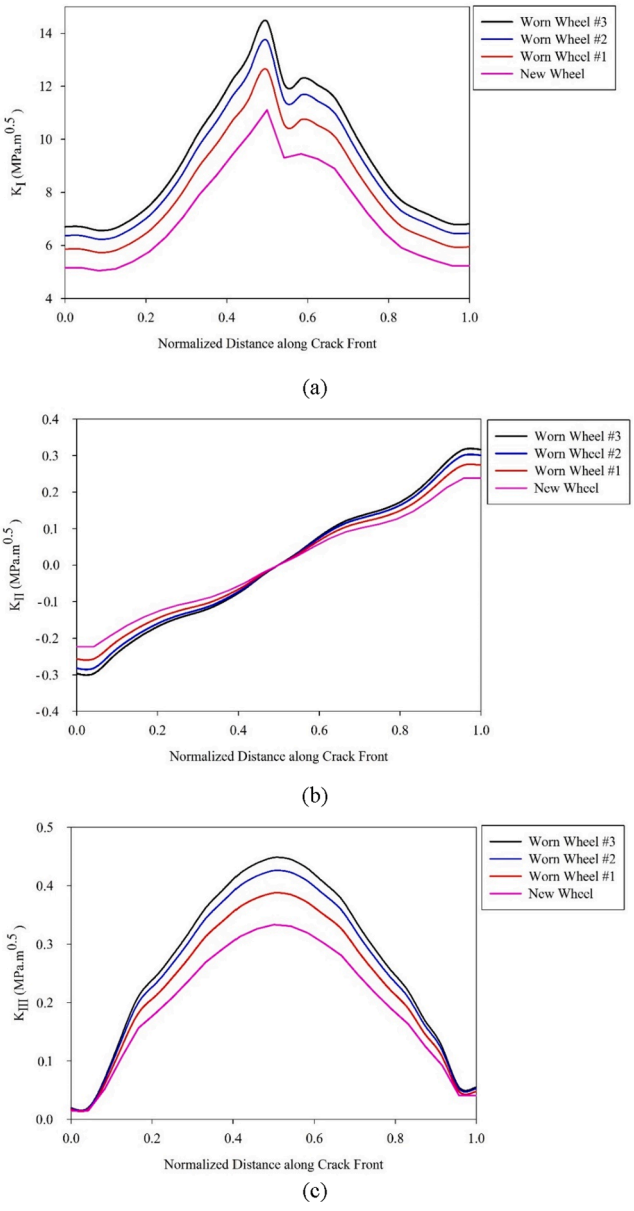

Fig. 6. SIFs according to normalized distance along crack front for different friction coefficients between wheel and rail for crack 1: (a) K_I, (b) K_{II}, and (c) K_{III}.

By integrating Eq. (5) in accordance with Eq. (2), the fatigue life is obtained [52]:

$$N = \int_{a_0}^{a_f} \frac{da}{C\beta^m \Delta\sigma^m (\pi a)^{\frac{m}{2}}}. \tag{6}$$

The geometric correction factor in Eq. (6) is the main and important parameter to obtain the stress intensity factor and the fatigue life. During the fatigue crack propagation of the web-frame structure, the geometric correction factor in Eq. (6) is the main and important parameter to obtain the stress intensity factor and the fatigue life. The ratio of the geometric correction factor for a crack is assumed an exponential-based function of a crack size as Eq. (7):

$$\beta = \frac{A}{\sqrt{a}} Exp(B.a) \tag{7}$$

where A and B are the regression parameters, which are considered to be Normal distributed random variables.

With Eqs. (6) and (7) we obtain:

$$N = \int_{a_0}^{a_f} \frac{da}{CA^m [Exp(B.a)]^m \Delta\sigma^m (\pi)^{\frac{m}{2}}}. \tag{8}$$

The service time for railway rail has been defined as Eq. (9):

$$t = \frac{N}{\upsilon}, \tag{9}$$

where $\upsilon$is the long-term average response frequency.

The long-term average response zero-crossing frequency can be calculated as Eq. (10) [53]:

$$\upsilon_0 = 1/[4log_{10}(L)], \tag{10}$$

where L is the length of ship.

With Eqs. (8) and (9), an explicit time variant expression for crack size can be presented as Eq. (11):

$$a(t) = -\frac{1}{Bm} ln\left[e^{-Bma_0} - BmCA^m \Delta\sigma^m \pi^{\frac{m}{2}} \upsilon_0 t\right] \tag{11}$$

The extent to which the crack length increases in each step can be calculated as Eq. (12):

$$a_i = a_{max}\left[\frac{K_I}{K_{I\,max}}\right]^b, \tag{12}$$

where, a_{max} is specified by the user in boundary element method.

In order to calculate the critical crack length, stress intensity factor of mode-I must be equal to fracture toughness. For this purpose, the stress intensity factor of mode-I is accorded against the fracture toughness values of fracture toughness tests to obtain the critical crack length in the railway rail. Therefore, we obtain:

$$a_f = \frac{K_C^2}{\pi\sigma_{max}^2 \beta^2}, \tag{13}$$

where, K_C is fracture toughness.

Based on probabilistic model of a crack growth as functions of time, the mean value and variance of the crack size are derived as [54]:

$$E[a(t)] = -\frac{1}{E(B)m} ln\left[e^{-E(B)mE(a_0)} - E(B)mE(C)E(A)^m E(\Delta\sigma)^m \pi^{\frac{m}{2}} \upsilon_0 t\right], \tag{14}$$

$$S^2[a(t)] = \left[\frac{\partial E[a(t)]}{\partial a_0}\right]^2 S_{a_0}^2 + \left[\frac{\partial E[a(t)]}{\partial \Delta\sigma}\right]^2 S_{\Delta\sigma}^2 + \left[\frac{\partial E[a(t)]}{\partial C}\right]^2 S_C^2 + \left[\frac{\partial E[a(t)]}{\partial A}\right]^2 S_A^2 + \left[\frac{\partial E[a(t)]}{\partial B}\right]^2 S_B^2, \tag{15}$$

The system fatigue reliability in this study is performed for five different crack lengths of both types of cracks (semi-elliptical crack and quarter-elliptical crack) discussed as a series system which can be seen in Fig. 1. After these five fatigue cracks initiated, four fatigue failure modes were defined at different locations for the Grade 900A rail steel.

The first mode is the fracture of the railhead because the sum of the crack lengths of crack 1 and crack 2 is larger than the dimension of the structural element containing crack 1 and crack 2. All other failure mode defined as: the complete fracture of crack 3, the complete fracture of crack 4 and the complete fracture of crack 5. Therefore, we obtain:

$$\begin{cases} a_1(t) + a_2(t) \geqslant a_{cr,1-2}, & if\ \ mod\ e = \text{First mode} \\ a_3(t) \geqslant a_{cr,3}, & if\ \ mod\ e = \text{Second mode} \\ a_4(t) \geqslant a_{cr,4}, & if\ \ mod\ e = \text{Third mode} \\ a_5(t) \geqslant a_{cr,5}, & if\ \ mod\ e = \text{Fourth mode} \end{cases} \tag{16}$$

For fatigue failure modes, the limit state function is written as:

$$g_i(t) = a_{cr,i} - a_i(t). \tag{17}$$

For first mode, $g_{1-2} = a_{cr,1-2} - a_1(t) - a_2(t)$ and fatigue failure will occur when $g_i(t) \leqslant 0$leading to$P_{f,i} = P(g_i(t) \leqslant 0)$, which may be evaluated by the standard normal distribution function as$P_{f,i} = \Phi(-\beta_i)$, where $\beta$is

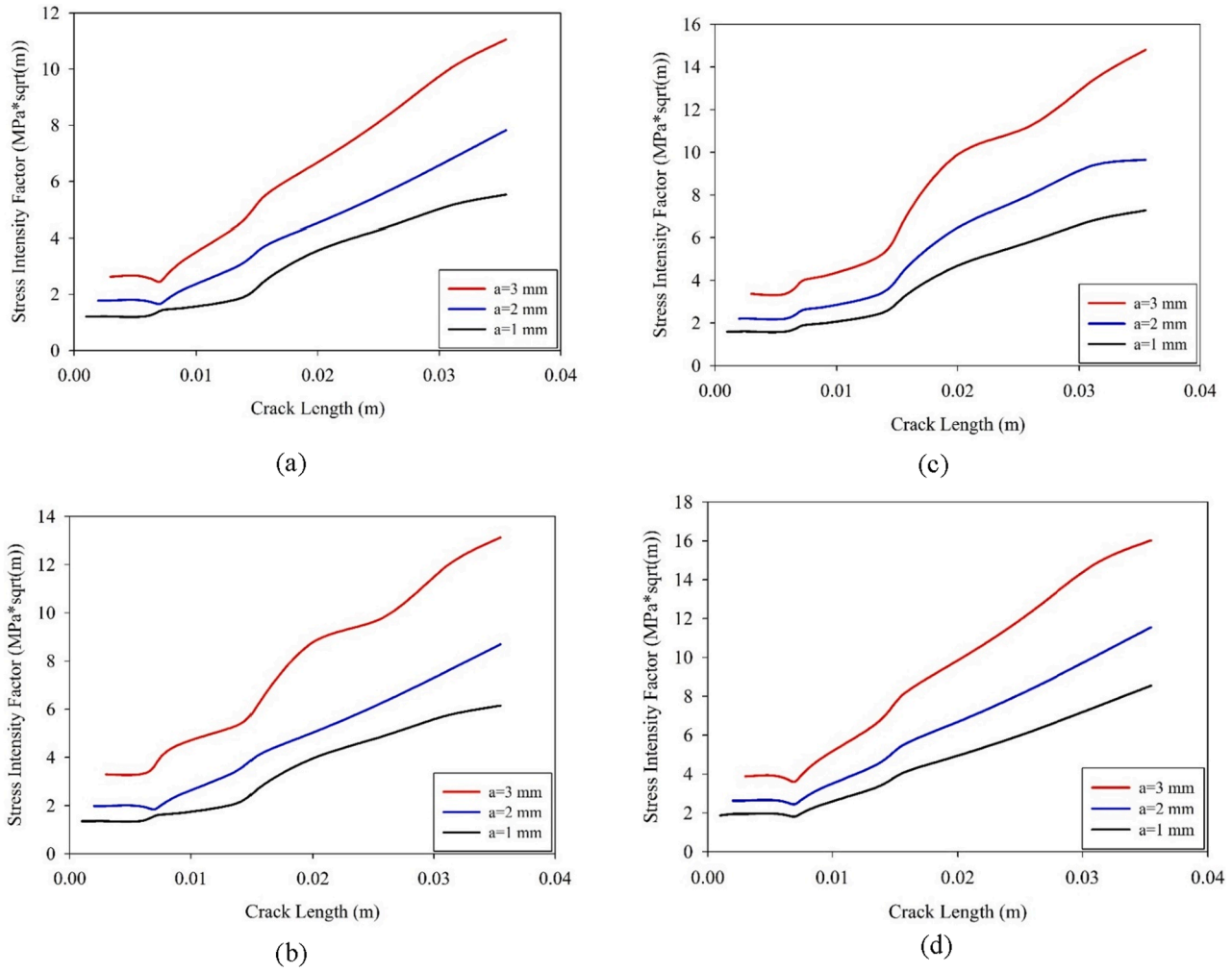

Fig. 7. SIF according to crack length for rail in contact with: (a) new wheel profile, (b) worn wheel #1, (c) worn wheel #2, and (d) worn wheel #3.

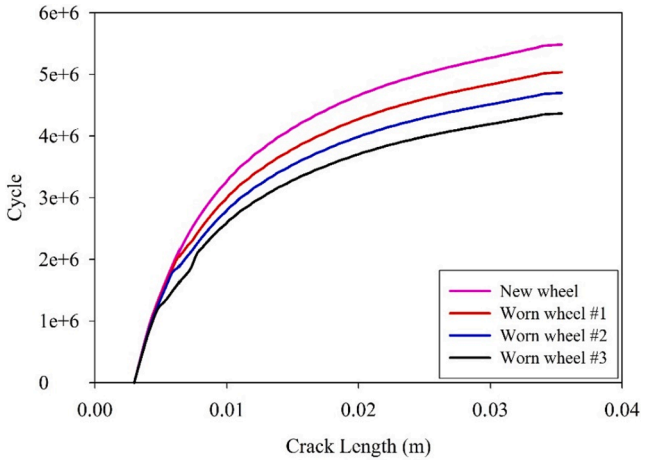

Fig. 8. Fatigue life against crack length for different S1002 wheel profile.

reliability index [55].

The reliability index of limit state function can be estimated as [55]:

$$\beta_i(t) = \frac{E|a_i(t)| - E|a_{cr,i}|}{\sqrt{\sigma^2_{a_i(t)} + \sigma^2_{a_{cr,i}}}}. \tag{18}$$

So, the fatigue reliability of limit state function for a Grade 900A rail steel is given as:

$$R_i(t) = \Phi[\beta_i(t)] \tag{19}$$

If the fatigue crack growth for a Grade 900A rail steel subjected to multiple cracks is considered independent, we obtain:

$$R_S(t) = R_S(t)\cdot R_S(t)\cdot R_S(t)\cdot R_S(t). \tag{20}$$

The Morgan law is used to describe the failure probability of the series system in accordance with Eq. (21) [55]:

$$\begin{aligned} P(U) &= P(U_1 \cup U_2 \cup U_3 \cup U_4) \\ &= \sum_{i=1}^{4} P(U_i) \\ &\quad - \sum P(\cap\text{Two components}) + \sum P(\cap\text{Three components}) + \ldots - P(U_1 \\ &\quad \cap U_2 \cap U_3 \cap U_4), \end{aligned} \tag{21}$$

The bounding techniques as the ‘‘narrow’’ bounds is also used to describe the failure probability as follow [56]:

$$\begin{aligned} P(U) &\geqslant P(U_1) + \sum_{i=2}^{4} max\left\{P(U_i) - \sum_{j}^{i-1} P(U_{ij}), 0\right\}, \\ P(U) &\leqslant \sum_{i=1}^{4} P(U_i) - \sum_{i=2}^{4} \underset{j<i}{max}\{P(U_{ij})\}, \end{aligned} \tag{22}$$

where,

Table 2
Mean value and standard deviation of the nonlinear regression models.

Crack No.	type of the wheel profile	Mean value for parameter A	Standard deviation for parameter A	Mean value for parameter B	Standard deviation for parameter B
Crack 1	New wheel	1.1209	0.5123	−0.0031	0.0001
Crack 2	New wheel	1.1045	0.4826	−0.0029	0.0001
Crack 3	New wheel	0.9563	0.1257	−0.0125	0.0002
Crack 4	New wheel	0.8254	0.2145	−0.0012	0.0005
Crack 5	New wheel	0.7198	0.3189	−0.0009	0.0002
Crack 1	Worn wheel #1	1.1324	0.5314	−0.0037	0.0001
Crack 2	Worn wheel #1	1.1259	0.4913	−0.0034	0.0001
Crack 3	Worn wheel #1	1.0896	0.1398	−0.0145	0.0003
Crack 4	Worn wheel #1	0.8725	0.2563	−0.0017	0.0005
Crack 5	Worn wheel #1	0.7602	0.3476	−0.0015	0.0003
Crack 1	Worn wheel #2	1.1628	0.5711	−0.0039	0.0002
Crack 2	Worn wheel #2	1.1523	0.5219	−0.0037	0.0002
Crack 3	Worn wheel #2	1.1147	0.1625	−0.0173	0.0003
Crack 4	Worn wheel #2	0.9124	0.2896	−0.0023	0.0006
Crack 5	Worn wheel #2	0.8188	0.3964	−0.0017	0.0003
Crack 1	Worn wheel #3	1.2536	0.6123	−0.0045	0.0002
Crack 2	Worn wheel #3	1.2312	0.5896	−0.0041	0.0002
Crack 3	Worn wheel #3	1.1817	0.2189	−0.0199	0.0003
Crack 4	Worn wheel #3	1.0236	0.33.28	−0.0029	0.0007
Crack 5	Worn wheel #3	0.9236	0.4511	−0.0025	0.0004

$$P(U_{ij}) = \Phi_2(-\beta_i, -\beta_j, \rho_{ij}) = \int_{-\infty}^{-\beta_1} \int_{-\infty}^{-\beta_2} \phi_2(x_i, x_j, \rho_{ij}) dx_i dx_j \tag{23}$$

and,

$$\phi_2(x_i, x_j, \rho_{ij}) = \frac{1}{2\pi\sqrt{1-\rho_{ij}^2}} exp\left\{ -\frac{1}{2} \cdot \frac{x_i^2 + x_j^2 - 2\rho_{ij}x_i x_j}{1-\rho_{ij}^2} \right\}, \tag{24}$$

where $\beta_i$and β_j are the reliability indices corresponding to the ith and jth component failure respectively, ρ_{ij} is the correlation coefficient between the ith and jth component failure.

The Ditlevsen solution is used to describe the bounding joint probability of failure for the series system in accordance with Eq. (25) [56]:

$$max\left\{ \Phi(-\beta_i)\Phi\left(-\frac{\beta_j - \rho_{ij}\beta_i}{\sqrt{1-\rho_{ij}^2}} \right), \Phi(-\beta_j)\Phi\left(-\frac{\beta_i - \rho_{ij}\beta_j}{\sqrt{1-\rho_{ij}^2}} \right) \right\} \leqslant P(U_{ij}) \leqslant \Phi(-\beta_i)\Phi\left(-\frac{\beta_j - \rho_{ij}\beta_i}{\sqrt{1-\rho_{ij}^2}} \right) + \Phi(-\beta_j)\Phi\left(-\frac{\beta_i - \rho_{ij}\beta_j}{\sqrt{1-\rho_{ij}^2}} \right) \tag{25}$$

3. Fatigue crack growth simulation

Studying fatigue and fracture of railway structure in the present investigation requires to find the crack initiation location by modeling wheel/rail contact in finite element method (FEM). For this purpose, the stress analysis of wheel/rail contact is performed using finite element method. In order to geometrically modeling of wheel and rail, the prominent profiles in railway applications named as S1002 and UIC60 are used, respectively. The new S1002 (for wheel) and UIC60 (for rail) profiles and three types of the worn wheel are defined according to [57]. The first, second and third worn profiles are measured at 200,000, 300,000 and 500,000 km, respectively [57]. Table 1 is also used for wheel and rail properties. variable amplitude service loading conditions is defined according to [11]. This load is the force caused by the rolling friction that enters the cracks and causes them to slip on each other. Due to the non-linearity of contact analysis, fixed boundary conditions are applied to the two ends of the rail. As shown in Fig. 2, the three-dimensional boundary element model is meshed for a Grade 900A rail steel. The boundary conditions in two sides of the rail are considered as clamped conditions. All other parameters such as material properties, boundary conditions, meshing and methods for the model are defined according to [50].

For modeling the fatigue crack, part of the rail between the two traverses is considered. Due to the symmetry of the rail, only half of this distance is modeled. According to Fig. 3 in the three-dimensional mode, a plate from the center of the rail under the maximum contact stress and assuming cracks in it due to the criticality of this plate is selected. Fig. 3 shows the boundary element model of the desired page and the crack in it, which has used more elements to achieve better results around the crack and the place of contact load. The load and dimensions of the elliptical contact surface created at the contact point of the wheel and rail are according to Hertz theory according to the Ref. [50]. The values of the stress intensity factors (SIFs) for the three different crack lengths of 1, 2 and 3 mm have been investigated. Also, the initial crack angle was selected according to field observations of 30°. Finally, by having the values of SIF, the direction of crack growth is also determined. Also, the fatigue crack propagation in each step is arbitrary. Once the crack growth direction is determined, the crack tip curve can be fitted and the crack can be grown for one step. After the crack grows, the rail is mesh again and is ready for solution. This is repeated for each step so that the crack grows as expected. For this study, the modified Paris model is used, which also considers the effects of fatigue crack closure. The fatigue crack growth rate based on this model is defined as Eq. (6). Fig. 3 shows the model of the rail with its cracks before segmentation. The initial crack length is 1 mm, 2 mm and 3 mm for each crack. In addition, the behavior of the material as elastic–plastic and the maximum tangential stress (MTS) crack extension criterion is used to obtain the fatigue crack growth path. In the numerical method, the crack tip for each crack is first divided into several elements. The displacement values obtained by the numerical method are calculated according to those SIFs. The stress analysis is performed via boundary element solver (BES) software. In addition to stress analysis for different loads, the values of SIFs were obtained. Then, two characteristics related to the fatigue crack growth, namely the crack growth and the fatigue crack growth path, have been calculated using these SIFs. Once the crack growth path is determined, the crack tip curve can be determined and

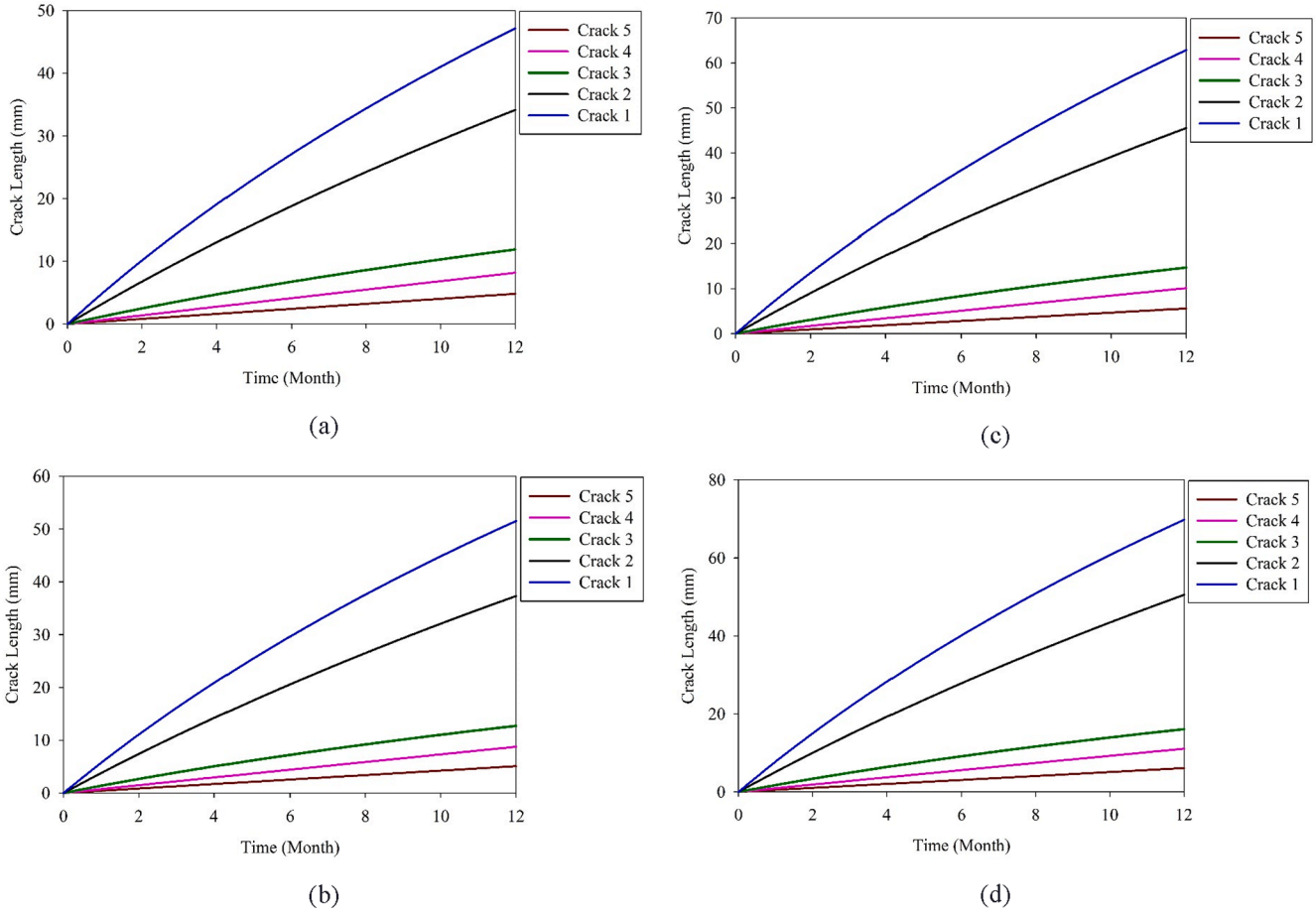

Fig. 9. Mean value of fatigue crack length in terms of time for five fatigue cracks during a 12-month anticipated service life: (a) new wheel profile, (b) worn wheel #1, (c) worn wheel #2, and (d) worn wheel #3.

the fatigue crack can be grown for one step. After that, material reconfigurate and preparing to calculate. This stage for every step repeated until expected growth for crack appear. Then fatigue crack growth under cyclic loading condition was modeled. Fig. 4 shows crack 1 and crack 2 after 14 stages. Finally, after inputting necessary data and calculation of stress intensity factor (SIF), the fatigue life for rail steel was calculated.

4. Results and discussion

4.1. Evaluation of fatigue crack growth

According to the results of finite element solution for wheel/rail contact, the maximum Von-Mises stress due to the contact of rail and new S1002 wheel is 509 MPa. The maximum value of Von-Mises stress for the contact of new rail and the first, second and third types of worn wheel profile are also computed as 509 MPa, 525 MPa, 556 MPa and 569 MPa, respectively (Fig. 5). These maximum values of stress are higher than the yield strength of steel and this comparison shows that the plastic zone occurs at the contact surface between wheel and rail.

Effect of geometry of wheel profile and the way it contacts to rail are also studied on stress intensity factors. Fig. 6 shows the SIFs at the crack tip against normalized distance along crack front. As can be seen in Fig. 6, wheel profile geometry and wheel/rail contact condition has significant effect on stress intensity factors and it is concluded that by selecting third type of worn wheel instead of new wheel, stress intensity factor of mode I is increased up to 22.9%.

Fig. 7 show the equivalent stress intensity factor in terms of crack length for different lengths of initial crack for crack 1 under the influence of contact with new railway wheel profile and the first, second and third types of worn wheel profile, respectively. According to Fig. 7-a, the SIF in steel rails has been increased from 1 mm to 2 mm about 29% and by changing the initial crack length from 1 mm to 3 mm about 49%. As can be seen in Fig. 7-b, the SIF increased from 1 mm to 2 mm to about 30% and from 1 mm to 3 mm by about 53%. According to Fig. 7-c by increasing the initial crack length, SIF will be increased, also when the initial crack length change from 1 to 2 mm, SIF increased about 24%. SIF by changing initial crack length from 1 to 3 increased about 51%. As can be seen in Fig. 7-d, the SIF increased from 1 mm to 2 mm to about 26% and from 1 mm to 3 mm by about 46%. Based on these results, the maximum SIFs belong to cracks with longer initial length. Also, the higher the wear of the railway wheel profile, the difference in the values of SIFs increases. Therefore, it can be concluded that in cyclic loading with increasing wear in railway wheel profile, crack growth intensity in rail increases. If the rail profile does not match the wheel due to the wear of the railway wheel profile, high stress filed are created until the rail is matched to the appropriate profile, so that the rail surfaces enters the plastic zone in the contact area. Therefore, it can be concluded that high wear rate can prevent the loss of primary cracks and their growth, but lower wear rate increases the time interval of continuation of high stresses and prevents this (loss of initial cracks).

In Fig. 8, the obtained fatigue life of railway rail in terms of critical crack length for crack 1 has been indicated due to the loadings applied from the new and three types of the worn wheel profiles. As can be seen in Fig. 8, the fatigue life reduced by changing the new wheel profile to worn wheel profile #1 about 9% and from new wheel profile to worn wheel profile #3 about 21%. Therefore, comparison of the obtained results showed that the effect of worn profile of railway wheel on fatigue life of steel rail is significant and cannot be ignored.

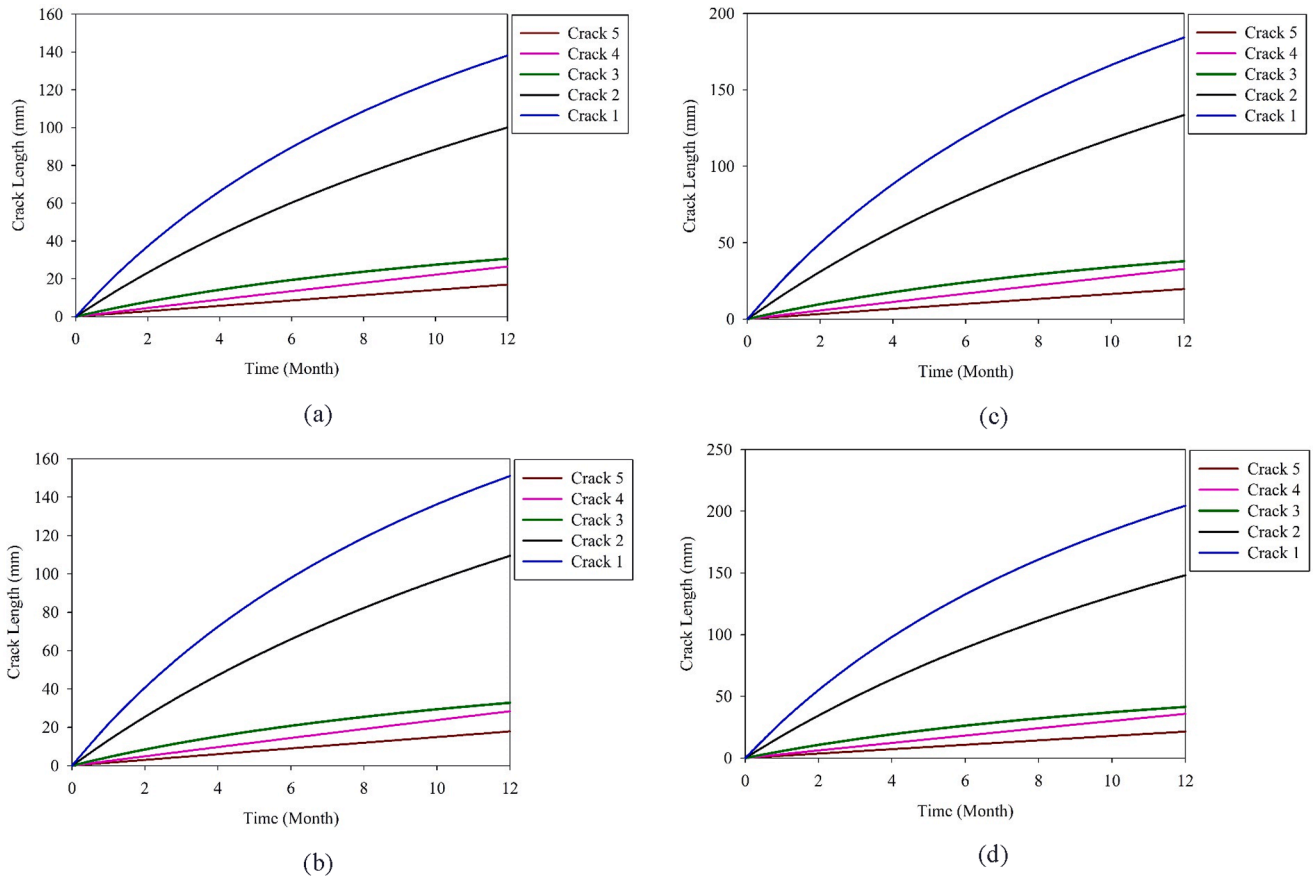

Fig. 10. Standard deviation of fatigue crack length in terms of time for five fatigue cracks during a 12-month anticipated service life: (a) new wheel profile, (b) worn wheel #1, (c) worn wheel #2, and (d) worn wheel #3.

4.2. Fatigue reliability assessment

Following the fatigue reliability analysis method in Section 2 and input parameters, a framework for the fatigue life estimation and fatigue reliability assessment was extended. For the fatigue reliability assessment of a Grade 900A rail steel during the design service life, the material parameter m is taken as 3.14 [36], the long-term average response zero-crossing frequency is assumed as 0.2 Hz, the design service life of a Grade 900A rail steel is taken as 12 months. The mean value and standard deviation of the nonlinear regression models for five cracks are listed in Table 2.

The comparison of the mean value of fatigue crack length during a 12-month anticipated service life for a Grade 900A rail steel in contact with the new and three types of the worn wheel profiles are shown in Fig. 9. As can be seen in Fig. 9, the relation between the fatigue crack length for each crack and service time is nonlinear. The mean value of the crack length for crack 1 are the longest one. Also, the mean value of the crack length for crack 5 are the smallest. As can be seen in Fig. 9, there is no significant difference between the mean value of the crack length for crack 1, crack 2, and crack 3. Also, the mean value of fatigue crack length increased by changing the new wheel profile to worn wheel profile #1 about 8% for crack 1 and from new wheel profile to worn wheel profile #2 and worn wheel profile #2 about 24% and 33%, respectively. Therefore, comparison of the obtained results showed that the effect of worn profile of railway wheel on crack length of steel rail is significant and cannot be ignored.

The comparison of the standard deviation of fatigue crack length during a 12-month anticipated service life for a Grade 900A rail steel in contact with the new and three types of the worn wheel profiles are shown in Fig. 10. The standard deviation of the crack length for crack 1 are the longest one. Also, the standard deviation of the crack length for crack 5 are the smallest. As can be seen in Fig. 10, there is no significant difference between the standard deviation of the crack length for crack 1, crack 2, and crack 3. Also, the standard deviation of fatigue crack length increased by changing the new wheel profile to worn wheel profile #1 about 9% for crack 1 and from new wheel profile to worn wheel profile #2 and worn wheel profile #2 about 25% and 32%, respectively.

Fig. 11 shows fatigue reliability assessment for four fatigue failure modes during a 12-month anticipated service life for rail steel in contact with the new and three types of the worn wheel profiles. As can be seen, there is no significant difference between second mode and third mode of failure for a Grade 900A rail steel. Also, the reliability assessments in terms of time for crack 5 (fourth mode of failure) are the highest value compared to other failure modes. It can be seen that the crack location has a significant effect on fatigue reliability for rail steel. The fatigue reliability, composed by crack 1 and crack 2 (first mode of failure), presents severe condition as already was indicated by the results of fatigue damage assessment. According to the results, the difference between the reliability results for the four failure modes is reduced by changing the new wheel profile to the worn wheel profile #3. Therefore, fatigue the reliability, composed by crack 4 (third mode of failure) in addition to crack 1 and crack 2 (first mode of failure) can present severe conditions for a Grade 900A rail steel in contact with worn wheel #3. It has to be pointed out the effect of fatigue damage for a Grade 900A rail steel has only to be accounted after the residual stress field due to mechanical contact is applied.

The system reliability assessment of rail steel in contact with the new and three types of the worn wheel profiles subjected to multiple cracks modelled as a series of components during a 12-month anticipated

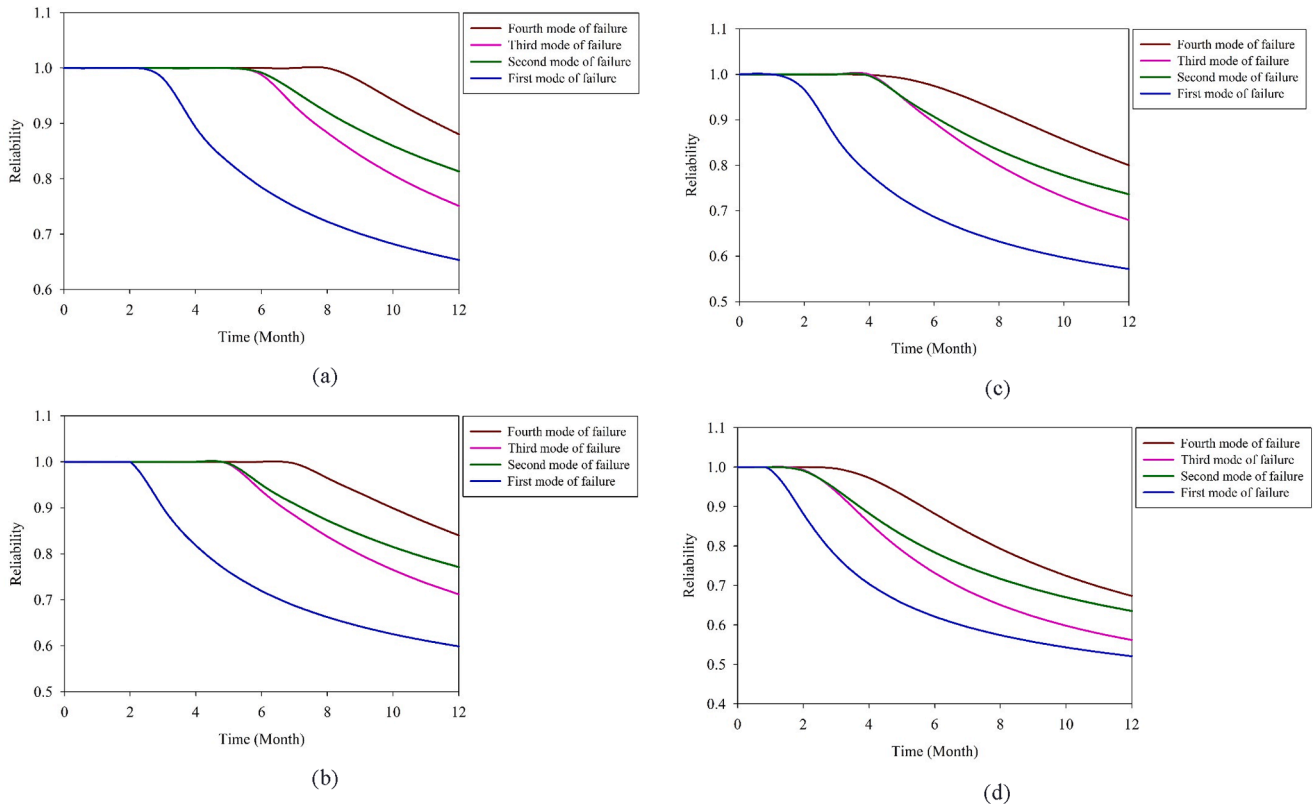

Fig. 11. Reliability assessments in terms of time for four failure modes: (a) new wheel profile, (b) worn wheel #1, (c) worn wheel #2, and (d) worn wheel #3.

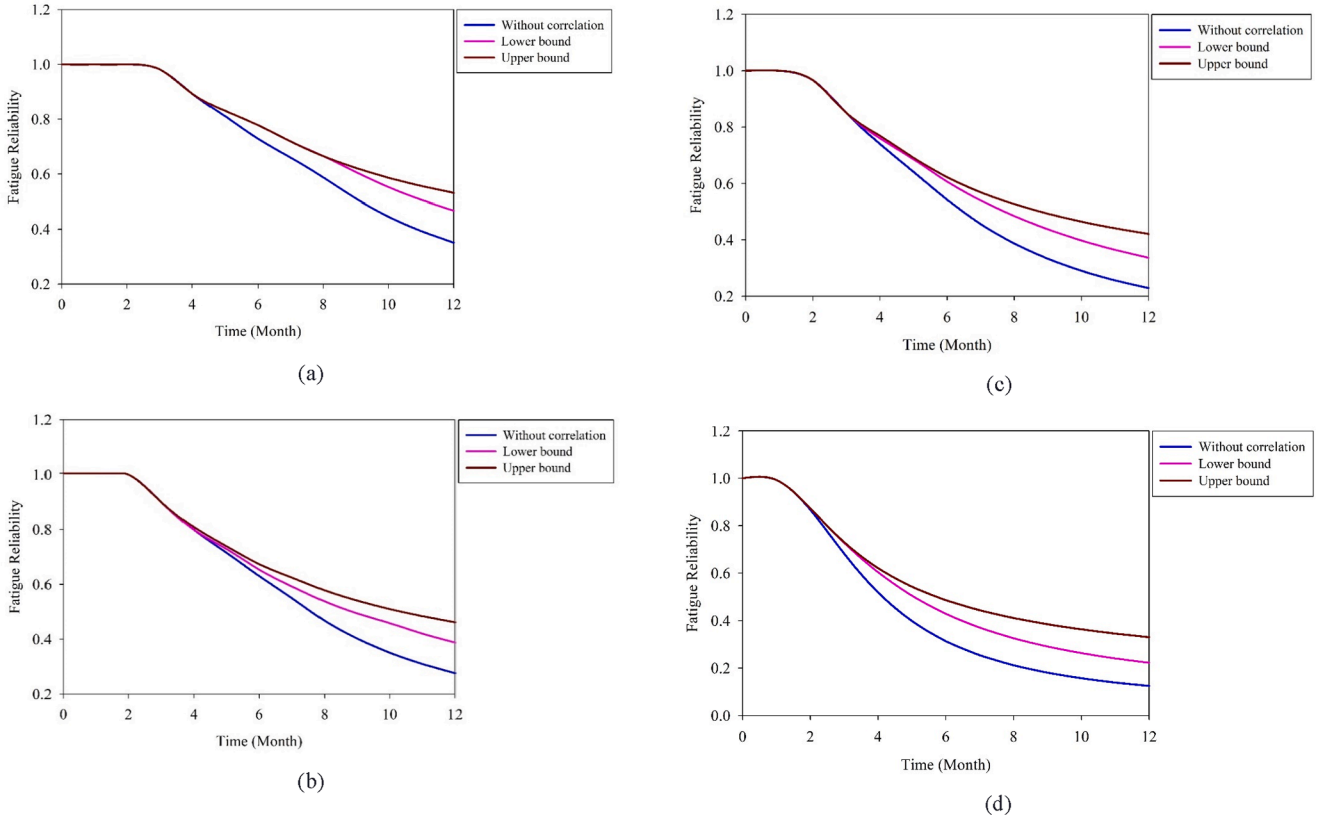

Fig. 12. Fatigue reliability of rail steel subjected to multiple cracks in terms of time: (a) new wheel profile, (b) worn wheel #1, (c) worn wheel #2, and (d) worn wheel #3.

service life and accounting for correlation is shown in Fig. 12. As can be seen, the lower bound of rail steel demonstrates lower reliability in comparison to the upper bound of rail steel. This is explained with the fact that the lower bound is related to a series system where the system components are fully correlated and the weakest element will dominate the system reliability. Here the crack 1 and crack 2 (first mode of failure) in rail surface, which is a surface of the rail steel, has the lowest fatigue reliability. Also, rail steel in contact with worn wheel #3 profile has the lowest fatigue reliability compared to rail steel in contact with the new and other two types of the worn wheel profiles. Also, the system reliability assessment of a Grade 900A rail steel subjected to multiple cracks modelled as a series of components during a 12-month anticipated service life and accounting for without correlation is demonstrated lower reliability in comparison to the upper bound and lower bound of rail steel. Also, this is explained that the fatigue reliability without correlation is related to a series system and the weakest element (first mode of failure) will dominate the system fatigue reliability assessment.

5. Conclusions

A new applied method for fatigue reliability assessment for a Grade 900A rail steel subject to the growth of multiple cracks under the influence of variable amplitude service loading conditions and wear was presented in this study. The results are based on the numerical method and using BEM. Stress intensity factors (SIFs) associated with three modes of fracture are calculated using the displacement approach. The rail steel modelled as a series system composed by the five cracks was evaluated based on the second order bounds. The geometry correction function of each crack has been developed. The results revealed that high wear rate can lead to initial crack elimination and prevent their growth, but low wear rate increases the time interval in which high stress field is applied and consequently has negative effect in elimination of initial cracks. Also, with increasing crack length, the SIFs of the surface crack tip also increase. The comparison of the fatigue life during the service life of 12 months showed that the fatigue life of crack 1 and crack 2 (first mode of failure) are highest, and crack 1 and crack 2 are the most critical for the structural integrity for a Grade 900A rail steel. Crack 1 and crack 2 are located in the rail head surface, so these cracks are the most critical cracks for rail steel. It is also observed that the stress intensity factor at tip of crack 1 and crack 2 is higher than other cracks, which indicates the importance of these cracks. In other words, the fatigue life for crack 1 and crack 2 are smaller than other cracks. The fatigue reliability, composed by crack 1 and crack 2 (first mode of failure) for rail steel in contact with worn wheel #3 profile, presents severe condition as already was indicated by the results of fatigue damage assessment. Also, the lower bound of rail steel demonstrates lower reliability in comparison to the upper bound of rail steel. This is explained with the fact that the lower bound is related to a series system where the system components are fully correlated.

Declaration of Competing Interest

The authors declare that they have no known competing financial interests or personal relationships that could have appeared to influence the work reported in this paper.

Acknowledgements

This work has been supported by the International Postdoctoral Exchange Fellowship Program (Talent-Introduction Program) of the P. R. China (Fund No. 234384), and the National Natural Science Foundation of China (Fund No. 61833002).

References

[1] Masoudi Nejad R, Farhangdoost Kh, Shariati M. Three-dimensional simulation of rolling contact fatigue crack growth in UIC60 rails. Tribol Trans 2016:1059–69.
[2] Lin TH, Ito YM. Mechanics of a fatigue crack nucleation mechanism. J Mech Phys Solids 1969;17(6):511–23.
[3] Lynch SP. A new model for initiation and growth of fatigue cracks. Metal Science 1975;9(1):401–10.
[4] Ekberg A, Kabo E, Andersson H. An engineering model for prediction of rolling contact fatigue of railway wheels. Fatigue Fract Eng Mater Struct 2002;25(10):899–909.
[5] Ciavarella M, Monno F, Demelio G. On the Dang Van fatigue limit in rolling contact fatigue. Int J Fatigue 2006;28(8):852–63.
[6] Ciavarella M, Monno F. A comparison of multiaxial fatigue criteria as applied to rolling contact fatigue. Tribol Int 2010;43(11):2139–44.
[7] Desimone H, Bernasconi A, Beretta S. On the application of Dang Van criterion to rolling contact fatigue. Wear 2006;260(4–5):567–72.
[8] Masoudi Nejad R, Shariati M, Farhangdoost Kh. Prediction of fatigue crack propagation and fractography of rail steel. Theor Appl Fract Mech 2019;101:320–31.
[9] Shariati M, Mirzaei M, Masoudi Nejad R. An applied method for fatigue life assessment of engineering components using rigid-insert crack closure model. Eng Fract Mech 2018;204:421–33.
[10] Masoudi Nejad R. Rolling contact fatigue analysis under influence of residual stresses. MS Thesis. Tehran: Sharif University of Technology, School of Mechanical Engineering; 2013.
[11] Masoudi Nejad R. Numerical study on rolling contact fatigue in rail steel under the influence of periodic overload. Eng Fail Anal 2020;115:104624.
[12] Masoudi Nejad R, Zhiliang L. Effect of periodic overloads and spectrum loading on fatigue life and microstructure in a Grade 900A rail steel. Theor Appl Fract Mech 2020;110:102796.
[13] Masoudi Nejad R. The effects of periodic overloads on fatigue crack growth in a pearlitic Grade 900A steel used in railway applications. Eng Fail Anal 2020;115:104687.
[14] Jung-Kyu K, Chul-Su K. Fatigue crack growth behavior of rail steel under mode I and mixed mode loadings. Mater Sci Eng, A 2002;338:191–201.
[15] Skyttebol A, Josefson BL, Ringsberg JW. Fatigue crack growth in a welded rail under the influence of residual stresses. Eng Fract Mech 2005;72:271–85.
[16] Beretta S, Boniardi M, Carboni M, Desimone H. Mode II fatigue failures at butt-welds. Eng Fail Anal 2005;12(1):157–65.
[17] Ekberg A, Åkesson B, Kabo E. Wheel/rail rolling contact fatigue – Probe, predict, prevent. Wear 2014;314(1–2):2–12.
[18] Afferrante L, Ciavarella M, Demelio G. A re-examination of rolling contact fatigue experiments by Clayton and Su with suggestions for surface durability calculations. Wear 2004;256(3–4):329–34.
[19] Clayton P, Su X. Surface initiated fatigue of pearlitic and bainitic steels under water lubricated rolling/sliding contact. Wear 1996;200:63–73.
[20] Liou HY, Wu WF, Shin CS. A modified model for the estimation of fatigue life derived from random vibration theory. Probab Eng Mech 1999;14:281–8.
[21] Shen H, Lin J, Mu E. Probabilistic model on stochastic fatigue damage. Int J Fatigue 2000;22:569–72.
[22] Susmel L, Hattingh DG, James MN, Tovo R. Multiaxial fatigue assessment of friction stir welded tubular joints of Al 6082–T6. Int J Fatigue 2017;101:282–96.
[23] Masoudi Nejad R, Tohidi M, Jalayerian Darbandi A, Saber A. Experimental and numerical investigation of fatigue crack growth behavior and optimizing fatigue life of riveted joints in Al-alloy 2024 plates. Theoretical Appl Fract Mech 2020;108:102669.
[24] G. Lesiuk, P. Kucharski, J.A.F.O. Correia, A.M.P.D. Jesus, C. Rebelo, L.S.d. Silva, Mixed mode (I + II) fatigue crack growth in puddle iron, Engineering Fracture Mechanics, Vol. In Press, pp. 2017.
[25] Masoudi Nejad R, Liu Z. Analysis of fatigue crack growth under mixed-mode loading conditions for a pearlitic Grade 900A steel used in railway applications. Eng Fract Mech 2021;247:107672.
[26] Masoudi Nejad R, Berto F, Tohidi M. Fatigue performance prediction of Al-alloy 2024 plates in riveted joint structure. Eng Fail Anal 2021;126:105439.
[27] Avontuur GC, Van der Werff K. An implementation of reliability analysis in the conceptual design phase of drive trains. Reliab Eng Syst Saf 2001;73(2):155–65.
[28] Jesus De, Abílio MP, et al. Fatigue assessment of a riveted shear splice based on a probabilistic model. Int J Fatigue 2010;32(2):453–62.
[29] Mohabeddine, Anis, José Correia, Pedro Aires Montenegro, Abílio De Jesus, José Miguel Castro, and Filippo Berto. "Probabilistic SN curves for CFRP retrofitted steel details." International Journal of Fatigue 148 (2021): 106205.
[30] Liao D, Zhu S, Correia JAFO, De Jesus AMP, Calçada R. Computational framework for multiaxial fatigue life prediction of compressor discs considering notch effects. Eng Fract Mech 2018;202:423–35.
[31] Zhu SP, Huang HZ, Peng W, Wang HK, Mahadevan S. Probabilistic Physics of Failure-based framework for fatigue life prediction of aircraft gas turbine discs under uncertainty. Reliab Eng Syst Saf 2016;146:1–12.
[32] Zhu SP, Hao YZ, Liao D. Probabilistic modeling and simulation of multiple surface crack propagation and coalescence. Appl Math Model 2020;78:383–98.
[33] Masoudi Nejad R, Berto F, Tohidi M, Jalayerian Darbandi A, Sina N. An investigation on fatigue behavior of AA2024 aluminum alloy sheets in fuselage lap joints. Eng Fail Anal 2021;126:105457.
[34] Schueller GI, Gasser M, Hartl J, Lener G. Practical design procedures using reliability based optimization. J. Adv. Manuf. Syst. 2001;4(1):101–20.

[35] Madsen, H., Sorensen, J.D., Olesen, R., "Optimal inspection planning for fatigue damage of offshore structures", in: A.-S. Ang, M. Shinozuka, G. Schueller, (Eds.), Proceedings of the Fifth International Conference on Structural Safety and Reliability (ICOSSAR'89), vol. 3, San Francisco, 2099–2106, 1989.
[36] Shoji H, Shinozuka M, Sampath S. A bayesian evaluation of simulation models of multiple-site fatigue crack. Probab Eng Mech 2001;16:355–61.
[37] Zhao J, Chan AHC, Roberts C, Madelin KB. Reliability evaluation and optimization of imperfect inspections for a component with multi-defects. Reliab Eng Syst Saf 2007;92:65–73.
[38] Peng, Xuan, Sivakumar Kulasegaram, S. C. Wu, and Stephane Pierre Alain Bordas. "An extended finite element method (XFEM) for linear elastic fracture with smooth nodal stress." Computers & Structures 179 (2017): 48-63.
[39] Wu SC, Peng X, Zhang WH, Bordas SPA. The virtual node polygonal element method for nonlinear thermal analysis with application to hybrid laser welding. Int J Heat Mass Transf 2013;67:1247–54.
[40] Adak Dibyendu, Pramod ALN, Ooi Ean Tat, Natarajan Sundararajan. A combined virtual element method and the scaled boundary finite element method for linear elastic fracture mechanics. Eng Anal Boundary Elem 2020;113:9–16.
[41] Teng ZH, Sun F, Wu SC, Zhang ZB, Chen T, Liao DM. An adaptively refined XFEM with virtual node polygonal elements for dynamic crack problems. Comput Mech 2018;62(5):1087–106.
[42] Brighenti Roberto. Application of the element-free Galerkin meshless method to 3-D fracture mechanics problems. Eng Fract Mech 2005;72(18):2808–20.
[43] Wu SC, Zhang SQ, Xu ZW. Thermal crack growth-based fatigue life prediction due to braking for a high-speed railway brake disc. Int J Fatigue 2016;87:359–69.
[44] Song Chongmin, Ooi Ean Tat, Natarajan Sundararajan. A review of the scaled boundary finite element method for two-dimensional linear elastic fracture mechanics. Eng Fract Mech 2018;187:45–73.
[45] Jiang Songwei, Yan Gu, Fan Chia-Ming, Wenzhen Qu. Fracture mechanics analysis of bimaterial interface cracks using the generalized finite difference method. Theor Appl Fract Mech 2021;113:102942.
[46] Masoudi Nejad R, Farhangdoost Kh, Shariati M. Microstructural analysis and fatigue fracture behavior of rail steel. Mech Adv Mater Struct 2020;27(2):152–64.
[47] Masoudi Nejad, R., 2017. "Three-dimensional analysis of rolling contact fatigue crack and life prediction in railway wheels and rails under residual stresses and wear". Ph. D. Thesis, Ferdowsi University of Mashhad, Mashhad.
[48] Aliakbari K, Imanparast M, Masoudi Nejad R. Microstructure and fatigue fracture mechanism for a heavy-duty truck diesel engine crankshaft. Scientia Iranica 2019; 26(6):3313–24.
[49] Masoudi Nejad, R., and Zhiliang L., 2020. "Effect of wear on stress intensity factor of rail steel using numerical modeling". In 3rd International Conference on Electrical, Computer and Mechanical Engineering, Iran.
[50] Masoudi Nejad R, Shariati M, Farhangdoost K. Effect of wear on rolling contact fatigue crack growth in rails. Tribol Int 2016;94:118–25.
[51] Masoudi Nejad R, Shariati M, Farhangdoost K, Atrian A. Rolling contact fatigue analysis of rails under the influence of residual stresses induced by manufacturing. Scientia Iranica 2018;26(3):1427–37.
[52] Stephens, R.I., Fatemi, A., Stephens, R.R., Fuchs, H.O., "Metal datigue in engineering", John Wiley & Sons Inc, Ed. 2, New York, 2001.
[53] Bach-Gansmo, O., C. A. Carlsen, and T. Moan. "Fatigue assessment of hull girder for ship type floating production vessels." Proceedings of the mobile offshore structure. Elsevier Science Limited, (1987).
[54] Soares, Guedes C, Garbatov Y. Reliability of maintained ship hulls subjected to corrosion and fatigue under combined loading. J Constr Steel Res 1999;52(1): 93–115.
[55] Huang W, Garbatov Y, Guedes Soares C. Fatigue reliability assessment of a complex welded structure subjected to multiple cracks. Eng Struct 2013;56:868–79.
[56] Ditlevsen O. Generalised second moment reliability index. Journal of Structural Mechanics 1979;7(4):435–51.
[57] Mahlooji V, Ghazavi MR. Railway vehicle derailment in curve due to wear. Modares Mechanical Engineering 2014;14(8):199–208.